

Characterization of a Continuous Wave Raman Laser in H₂

J. K. Brasseur, P.A. Roos, K. S. Repasky and J.L. Carlsten
Department of Physics
Montana State University
Bozeman MT., 59717

e-mail: carlsten@physics.montana.edu

Abstract:

In this paper we present a time-dependent theory that describes the continuous wave (cw) Raman laser in H₂. The time-dependent theory is compared to existing theories and threshold measurements are taken. The relative intensity noise of the pump and Stokes beams is measured and found to be in agreement with the predictions of the presented theory. The Raman laser decreases the relative intensity noise of the pump beam by 34dB/Hz at a frequency of 30kHz. In addition the spectral heterodyne beat-note linewidth of the continuous wave Raman laser is measured to be 8kHz.

OCIS numbers:140.3550, 190.5650, 290,5910, 290.5860

Introduction

Recent experimental [1,2] and theoretical [2,3] studies have been conducted in non-resonant Raman scattering using a continuous wave (cw) laser pump source. These studies have been made possible by developments in mirror coating technology which have led to the availability of low loss, high reflectivity mirrors. With reflectivities approaching 99.995% for multiple wavelengths, high finesse cavities (HFCs) can be constructed with finesses of 50,000 and higher [4,5]. When resonant, the circulating power inside a HFC is roughly the finesse times the optical power at the entrance of the cavity. Thus, stimulated Raman scattering can be studied with relatively low power cw lasers.

Raman scattering occurs when an incident photon interacts with a molecule (or an atom) and generates a red-shifted photon (Stokes) resulting from the conservation of energy when the excitation in the molecule occurs. The molecular excitation can be vibrational, rotational, or electronic. In references 1-3 non-resonant vibrational Raman scattering in H₂ was studied, and thresholds on the order of a milli-watt were observed. With low cost diode lasers, cw Raman lasers covering the spectrum from the visible to the near IR (~4 μ m) are possible.

Possible applications of the cw Raman laser will be in laser frequency synthesis and high-resolution spectroscopy. Two attributes that were not discussed in references 1-3 but are critical to the applicability of the source are its spectral purity and amplitude noise. In this paper we address the amplitude noise of the cw Raman laser both experimentally and theoretically. In addition the spectral linewidth and stability of the source are measured.

This paper is organized in the following manner. Section 2 develops the time-dependent cw Raman laser equations. Section 3 examines the steady-state limits of these equations and compares the results to previous theories. Section 4 solves the time-dependent equations to predict the temporal dynamics of the cw Raman laser as seen by relaxation oscillations as well as the relative intensity noise (RIN). Section 5 provides the experimental verification of the time dependent theory. Section 6 studies the free-running linewidth of the cw Raman laser. Section 7 contains some concluding remarks, and an appendix is provided to discuss the particular difficulties in phase/frequency locking of the pump laser to the Raman cavity due to the Raman process.

2. Time-dependent Raman Laser Equations

Theoretical studies have been conducted predicting the effects of using a non-classical pump source for a non-resonant cw Raman laser [6]. These studies predict that a photon number squeezed pump source will produce a photon number squeezed Stokes output. In addition, preliminary theoretical studies have been performed on a cw Raman in H_2 [2,3,7]. However, the theories presented in references 2,3 and 7 are steady-state theories which lack the time dependence to predict the relaxation oscillations seen at high pump powers in references 1 and 2.

Behavior seen in a quasi-cw Raman laser in NH_3 has been described mathematically [8]. Using the equations derived in reference 8 with the additional assumptions that the time rate of change of the population is zero and the coherence between the ground and vibrational state is well established [9], we arrive at an equation that describes the growth of the Stokes field. However, the assumption that the pump

field is not depleted is no longer valid, so a pump equation also needs to be included. This is done similar to the method outlined in references 2 and 8 with optical pumping phenomenologically added. To further simplify the equations, the pump and Stokes fields are assumed to be resonant with the optical cavity. As a result we have the following time dependent equations which describe fields inside the Raman laser cavity.

$$\dot{E}_p = -L_p E_p - \frac{\omega_p}{\omega_s} G |E_s|^2 E_p + K(E_{p_m}, t) \quad (1)$$

$$\dot{E}_s = -L_s E_s + G |E_p|^2 E_s \quad (2)$$

E_p (E_s) is the pump (Stokes) field, and ω_p (ω_s) is the pump (Stokes) frequency. The losses due to the mirrors at the pump (Stokes) frequency are given by L_p (L_s). The gain of the Raman system is given by G , and the cavity is optically pumped by $K(E_{p_m}, t)$ where E_{p_m} is the pump field incident on the HFC. The Raman gain, G , for the Stokes field is [10]:

$$G = \frac{1}{2} \left(\frac{1}{8} \alpha \cdot c \sqrt{\frac{\epsilon_0}{\mu_0}} \left(\frac{2\lambda_p}{\lambda_p + \lambda_s} \right) \right) \quad (3)$$

where α is the plane-wave gain coefficient and c is the speed of light, $2\lambda_p/(\lambda_p + \lambda_s)$, is a mode filling parameter which accounts for the focusing of the beams where $\lambda_{p(s)}$ is the wavelength of the pump (Stokes) beam [11]. A standing wave is formed inside the HFC instead of a traveling wave, so a spatial average was performed that reduced the gain by a factor of 2 [12]. By setting G and $K(\omega, t)$ equal to zero in equations 1 and 2, we arrive at the following expression for mirror losses L_p and L_s .

$$L_{p(s)} = -\frac{c}{2\ell} \ln \sqrt{R_{p(s)_f} R_{p(s)_b}} \quad (4)$$

where ℓ is the length of the cavity and $R_{p(s)f(b)}$ is the reflectivity of the front (back) mirror at the pump (Stokes) wavelength. To determine the optical pumping constant, $K(E_{p_{in}}, t)$, we set the gain, G , equal to zero in equation (1). We then solve the inhomogeneous differential equation with the appropriate boundary conditions. This results in $K(E_{p_{in}}, t)$ taking the following form [13]:

$$K(E_{p_{in}}, t) = \frac{c}{\ell} \sqrt{T_{p_f}} E_{p_{in}} \quad (5)$$

where the transmission of the front mirror at the pump wavelength, T_{p_f} , is needed to write equation (5) in terms of $E_{p_{in}}$. Figure-1 shows the results of numerically integrating the Raman laser equations 1 and 2 [14]. The pump field inside the cavity increases with time until the threshold of the Raman laser is reached. The Stokes field then grows and a relaxation oscillation is observed which is damped rapidly. The steady-state values for the pump and the Stokes fields are then reached.

3. Steady-State limit of Raman Laser Equations

In the steady state, equations 1 and 2 are set to zero, and we solve for the pump and Stokes fields. This results in the following expressions for the steady-state pump field, $E_{p_{ss}}$, and Stokes field, $E_{s_{ss}}$ inside the Raman cavity,

$$E_{p_{ss}} = \sqrt{\frac{L_s}{G}} \quad (6)$$

$$E_{s_{ss}} = \sqrt{\frac{\omega_s (K - L_p E_p)}{\omega_p G E_p}}. \quad (7)$$

Equation 6 is independent of the pumping constant, K , so once the cw Raman laser threshold is reached the pump power inside the HFC remains constant. The threshold

occurs when the Stokes field amplitude becomes real valued ($K=L_p E_p$). Using equations 5-7 we can express the required pump field incident on the Raman cavity for threshold as:

$$E_{p_{in,thres}} = \frac{\ell L_p}{c} \sqrt{\frac{L_s}{T_{p_f} G}}. \quad (8)$$

To find the fields outside of the Raman cavity we multiply by $\frac{1}{2}\sqrt{T}$ since light can escape from either of two mirrors. The fields exiting the HFC therefore take the following form.

$$E_{p_{ssf}} = -\sqrt{R_{p_f}} E_{p_{in}} + \frac{1}{2}\sqrt{T_{p_f}} E_{p_{ss}} \quad (9a)$$

$$E_{p_{ssb}} = \frac{1}{2}\sqrt{T_{p_b}} E_{p_{ss}} \quad (9b)$$

$$E_{s_{ssf}} = \frac{1}{2}\sqrt{T_{s_f}} E_{s_{ss}} \quad (10a)$$

$$E_{s_{ssb}} = \frac{1}{2}\sqrt{T_{s_b}} E_{s_{ss}} \quad (10b)$$

where the first term on the right side of equation 9a accounts for the reflected incident pump field. While expressions 9-10 do not explicitly show a dependence on absorptions and scattering losses, the expressions do depend on the R (reflectivity) and the T (transmission) of the mirrors, and these values must satisfy $R+T+A=1$. Thus, the absorption dependence is implicit in the expressions.

The pump and the Stokes fields can be converted into powers by the following equation:

$$\Pi = \frac{1}{2} \sqrt{\frac{\epsilon_0}{\mu_0}} |E|^2 A \quad (11)$$

with the scaled area, A , for both the pump and the Stokes fields given by [11,15]:

$$A = \frac{\ell \lambda_p}{4 \tan^{-1}\left(\frac{\ell}{b}\right)} \quad (12)$$

where ℓ is the length of the cavity and b is the confocal parameter of the beam. Figure-2 shows the predictions of equations 9-10 with the predictions of references 2 and 3 overlaid [14]. We see that the steady-state predictions of the current theory are in good agreement with previous steady-state theories.

4. Relaxation oscillations and Relative Intensity Noise (RIN)

Figure-1 shows the relaxation oscillation damping out in the absence of noise to drive the oscillation. To see the effect of intensity noise on the output of the cw Raman laser a noise term is added into equation 1, giving the following modified cw Raman laser equations:

$$\dot{E}_p = -L_p E_p - \frac{\omega_p}{\omega_s} G |E_s|^2 E_p + K(1 + \beta \sin(\omega t)) \quad (13)$$

$$\dot{E}_s = -L_s E_s + G |E_p|^2 E_s \quad (14)$$

where ω is the angular frequency of the noise and β is the amplitude of the oscillation relative to the incident pump field. These equations are numerically integrated for various pump powers and angular noise frequencies allowing for calculation of the amplitude noise.

The amplitude noise of a laser is commonly expressed in terms of RIN. Noise predicted by equations 13 and 14 is converted to RIN according to the following equation:

$$RIN_{output} = 40 \cdot \text{Log}_{10} \left(\frac{\delta E_{rms}}{E_{ss}} \right). \quad (15)$$

where δE_{rms} is the field RMS noise and E_{ss} is the steady-state value of the field at the output of the cw Raman laser.

Since the HFC can add noise via converting frequency deviations into intensity noise, the RIN_{output} of the pump and Stokes beams were normalized to the pump RIN at the exit of the HFC below threshold for measurement purposes. Thus the normalized RIN for the pump (Stokes) is given by:

$$\Delta_{P(S)} = RIN_{output_{P(S)}} - 40 \cdot \text{Log}_{10}(\beta_{rms}) - 20 \log_{10}(C_p(\omega)) \quad (16)$$

where $\beta_{rms} = \frac{\beta}{\sqrt{2}}$ and $C_p(\omega)$ is the frequency response of the HFC for the pump beam.

Therefore, the normalized RIN of the pump (Stokes) beam, $\Delta_{P(S)}$, allows for general statements about the reduction or addition of amplitude noise by just the Raman process.

The functional dependence of Δ_p and Δ_s on the noise frequency, $\frac{\omega}{2\pi}$, is calculated by using equations 13-16 [14].

Figure 3 shows the results of this calculation for the normalized RIN of the pump (Stokes), $\Delta_{P(S)}$, for a pump power of four times the threshold of the Raman laser. The normalized RIN of the Stokes beam, Δ_s , is seen to increase up to a noise frequency of 125kHz where the relaxation oscillation frequency is reached. Furthermore, for noise frequencies above the relaxation oscillation frequency, the response of the HFC at the Stokes wavelength reduces Δ_s . The Stokes RIN at the relaxation oscillation frequency is seen to be 17 dB/Hz larger than the input pump RIN.

The calculated normalized RIN of the pump beam, Δ_p , is also shown in figure 3. Due to the self-limiting nature of the pump beam (equation 6), Δ_p is expected to decrease with respect to the input pump beam. However, the medium has a resonance due to relaxation oscillations, seen in Δ_s of figure 3, which causes an increase in Δ_p near the relaxation oscillation resonance. Thus, for noise frequencies below the relaxation oscillation resonance, Δ_p initially increases with the noise frequency until the relaxation oscillation is reached, then Δ_p levels off for larger noise frequencies as shown in figure-3.

Figure 4 shows the calculated dependence of the relaxation oscillation frequency on pump power of the Raman laser. The relaxation oscillation frequency is calculated by solving equations 13-16 for various pump powers and selecting the frequency corresponding to the maximum of Δ_s . The relaxation oscillation frequency of the Raman laser is seen to increase with pump power, but increases much more slowly when it reaches the Stokes cavity linewidth. The Stokes cavity linewidth is reached at a pump power of approximately four times threshold. For large pump powers, the relaxation oscillation frequency levels off to approximately twice the Stokes cavity linewidth.

5. Experimental Apparatus

Figure-5 shows the experimental apparatus used to measure the threshold, and RIN of the cw Raman laser. The device was pumped by a frequency doubled Nd:YAG with output powers up to 200mW. The output of this Nd:YAG laser was at 532nm and was sent through two faraday isolators to minimize feedback to the Nd:YAG laser. The beam was then passed through a resonant phase modulator to place sidebands on the carrier frequency required for phase/frequency locking of the cavity and the pump beam. An

electro-optic modular (EOM) in conjunction with an acousto-optic modular (AOM) provided external phase/frequency tuning of the laser frequency [16]. A half-wave plate with a downstream polarizing beamsplitter (PBS) provided a variable pump power. The beam then traveled through a two-element lens pair to mode match the pump beam to cavity. A PBS in conjunction with a quarter-wave plate allowed for the monitoring of the reflected beam for phase/frequency locking. A fast photo-detector was used to measure the error signal. A low-noise amplifier gave the signal 30dB of gain before it was mixed to dc. The error-signal entered the servo, which sent the slow corrections (DC-1kHz) to a piezo-electric transducer (PZT) used to control the spacing of the HFC mirrors. The intermediate frequencies were sent to the AOM (10Hz-180kHz), while the fast corrections were sent to the EOM (DC-800kHz). A small portion of the beam was diverted by a glass slide to monitor the pump power at the front of the cavity. A prism was used to spatially separate the pump (532nm) and the Stokes (683nm) beams at the exit of the cavity. The photo-detector signals were split. The dc signals were sent to digital voltmeters to measure the output powers while the ac signals (>10Hz) were given a transimpedance gain of 30dB and the RINs of the pump and Stokes beams were measured by RF spectrum analyzers.

Figure 6 shows the output Stokes power as a function of input pump power, and figure 7 shows the photon conversion efficiency as a function of pump power. The threshold of the cw Raman laser is $640 \pm 30 \mu\text{W}$ [17], and the maximum conversion efficiency is $27 \pm 3\%$ at 2.6mW of pump power [18]. The theoretical fit was obtained using equations 9-10 and using mirror reflectivities (transmissions) of 0.99980 (156ppm) and 0.99977 (163ppm) for the pump and Stokes wavelengths, respectively [19]. The

Raman cell was filled to 10atm. with H₂ which gave a Raman linewidth of 510MHz (FWHM) [20]. The cavity length was 7.68cm, the radius of curvature of the mirrors was 25cm, and $\alpha = 3.45 \times 10^{-9}$ cm/W [21]. Deviations from the theoretical fits at larger pump powers may be caused by distortions in the HFC mirrors. Such distortions can result from thermal heating by the absorption of the high optical power circulating in the HFC.

Figure-8 shows the pump RIN before and after the HFC with the calculated shot noise level for reference. The pump RIN after the HFC is larger for two reasons: the AOM steers the beam slightly which changes the coupling efficiency, and the HFC converts frequency noise into amplitude noise. Thus, we normalize the pump and the Stokes RIN to the pump RIN at the exit of the cavity below threshold. The pump and Stokes RIN were measured at every data point of the threshold curve.

Figures-9a and 9b show the normalized RIN of the Stokes and pump beams at four times the threshold of the Raman laser. The theoretical normalized RIN fits were obtained using equations 13-16 and the parameters of the threshold fits [14]. Both the Stokes and pump fits are in agreement with predictions of the theory. The significant deviations in Δ_p seen in the frequency range of 0 to 20kHz are caused by instabilities in the PZT servo. In addition, for larger pump powers (6 times threshold and larger) the phase/frequency locking system prohibited consistent measurements of the RIN at frequencies above the pump cavity half-width (64kHz). Appendix A addresses the difficulties in the phase/frequency locking at these high pump powers.

Figure-10 shows the normalized RIN of the pump and the Stokes beams at frequency of 30kHz as a function pump power. For small pump powers the normalized RIN for the Stokes was 30dB/Hz, and reduced to -5dB/Hz at higher pump powers. The

normalized pump RIN was reduced to -34dB/Hz for large pump powers, which was 45dB/Hz above the calculated shot noise level. The theoretical RIN fits were obtained using equations 13-16 and the parameters of the threshold fits [14]. The fits show that the predictions of the theory for frequencies below the cavity half-width (64kHz) are valid for all pump powers.

6. Cw Raman Laser Linewidth

Two identical cw Raman lasers were constructed to measure the free running laser linewidth of the device. A simplified experimental diagram is shown in figure-11. The locking servo was identical to that of figure-5; however, the EOM for phase control was absent [22]. Emissions from the two Raman lasers were overlapped and a RF spectrum analyzer and a precision frequency counter measured the beat signal. Figure 12 shows the spectrum analyzer output for a 10ms sweep. The FWHM of the beat signal was measured to be 8kHz in a resolution bandwidth of 2.9kHz. The Schawlow-Townes laser linewidth is ~10mHz for the cw Raman laser. Deviations from this limit were caused by vibrations experienced by the HFC [23] and were not due the Raman process. Thus, for a well isolated HFC the cw Raman laser beat-note linewidth should reach the 10-100Hz level.

The stability of the cw Raman laser was studied by measuring the Allan-variance. The Allan-variance of the beat frequency is shown in figure-13, which was calculated for a sample size of 100 for integration times of 10 seconds and smaller had a sample size of 20 for the 100 second integration time. The Allan-variance had a peak at ~100Hz caused by vibrations present on the optical table [23]. The Allan-variance had a minimum of 1kHz at an integration of ~1 second before long term cavity drifts took over.

7. Conclusions

The threshold of the cw Raman laser was measured to be $640 \pm 30 \mu\text{W}$. A time-dependent theory that describes the cw Raman laser was presented. The steady-state limit of the theory agrees well with existing theories. The theory also predicts the relaxation oscillations observed in references 1 and 2. The theory predicts the structure of the RIN for both the pump and the Stokes beams which is in agreement with experimental results. The heterodyne beat-note linewidth was measured to be 8kHz in a resolution bandwidth of 2.9kHz.

Appendix A Phase/Frequency stability requirements.

In order to construct the stable, low amplitude noise cw Raman laser described in this paper the following two criteria had to be met. The servo bandwidth needed to be larger than the HFC linewidth due to intensity dependent changes of the index of refraction associated with the Raman process, and the amount of dc gain needed to be larger than expected due to the self-limiting of the pump intensity inside of the HFC.

For the high pump and Stokes intensities inside the HFC, intensity dependent changes in the index of refraction occur. This index change affects the phase of the reference beam created by the HFC used in optical locking, so oscillations in the pump or the Stokes beams create oscillations in the error signal. Relaxation oscillations are the predominate source for intensity noise for the cw Raman laser which occur at frequencies at or slightly larger than the cavity linewidth. If the bandwidth of the servo controlling the system is smaller than the cavity linewidth, the relaxation oscillation is actually driven by the control electronics. Therefore, the bandwidth of the servo needed to be

larger than the cavity linewidth for the relaxation oscillations to be reduced to the predictions of the theory.

The self-limiting nature of the pump intensity inside the HFC once the Raman laser lases presents an additional locking difficulty. The noise of a laser is traditionally separated into two regimes: frequency (noise slower than the HFC half-width) and phase (noise faster than the HFC half-width) noise. As the pump rate of the Raman laser is increased so does the size of the error-signal in the phase regime. However, the error signal in the frequency regime remains constant due to the self-limiting. Traditionally when a laser is locked to a reference cavity the gain of the servo (feedback) is increased until instability arises, then the gain is reduced slightly. For the Raman process, the instability occurs in the phase regime of the noise, so as the pump rate is increased, the gain of the servo must be decreased to maintain closed-loop stability. However, the reduction of the gain from the servo decreases the error-signal in the frequency regime, reducing the long-term frequency stability of the Raman laser. This effect becomes significant for larger pump rates; for example, operating the Raman laser at 10 times threshold the dc gain is reduced by 20dB. A solution is to add more dc gain below the cavity linewidth via a compensated integrator with a corner inside the cavity half-width.

Acknowledgments:

This work is supported by a National Science Foundation grant PHY-9731602. We thank Jan Hall and his group at JILA and Michael Jefferson at IBM for their help.

References

- [1] J. K. Brasseur, K. S. Repasky, and J. L. Carlsten, *Opt. Lett.* **23**, 367 (1998).
- [2] K. S. Repasky, J. K. Brasseur, L. Meng, and J. L. Carlsten, *J. Opt. Soc. Am. B*,

- 15**, 1667 (1998).
- [3] K. S. Repasky, L. Meng, J. K. Brasseur, J. L. Carlsten, and R. C. Swanson, accepted for publication in *J. Opt. Soc. Am. B*, (1999)
- [4] K. S. Repasky, L. E. Watson, and J. L. Carlsten, *Appl. Opt.* **34**, 2615 (1995).
- [5] K. S. Repasky, J. G. Wessel, and J. L. Carlsten, *Appl. Opt.* **35**, 609 (1996).
- [6] S. Rebic, A. S. Parkins, and D. F. Walls, *Optics Commun*, **156**, 426 (1998).
- [7] P. Peterson, A. Gavrielides, M. P. Sharma, *Optics Commun*, **160**, 80 (1999).
- [8] R. G. Harrison, Weiping Lu, and P. K. Gupta, *Phys. Rev. Lett.* **63**, 1372 (1989).
- [9] \dot{D}_{13} and $\dot{\rho}_{31}$ from reference 8 are set to zero. The population difference of the ground state and the vibration state is assumed to be 1, due to the fact that in 10 atm. of H₂ only ~ 1 molecule in 10⁴ of the molecules available participate in the Raman process. In addition, the Raman linewidth is on the order of 510MHz for 10 atm. of H₂ which gives a coherence decay of ~2ns, while the Raman cavity has a build up time ~1-10μs, so coherence effects can be ignored.
- [10] D. C. Mac Pherson, R. C. Swanson, and J. L. Carlsten, *J. of Quantum Electron.* **25**, 1741 (1989).
- [11] G. D. Boyd, W. D. Johnston, and I. P. Kaminow, *J. of Quantum Electron.*, **QE-4**, 203 (1969).
- [12] For our system the gain per pass of the Stokes beam is $\sim 1 \times 10^{-4}$, so the gain of the system can be treated as if it were linear ($\exp(G) \rightarrow 1+G$), so a spatial average of the pump's field inside the Raman laser cavity is sufficient to calculate the gain. The spatial average reduces the gain by a factor of 2. This factor of one half is absent in References 1 and 2 and should be included.

- [13] We have an inhomogeneous differential equation, which is solved by a linear combination of the homogeneous solution and the particular solution such that the following boundary conditions are met. At time equal to zero the pump inside of the cavity is zero, and at time equal to infinity our solution limits to $\frac{\sqrt{T}}{1 - \sqrt{R}}$, the result of a discrete sum of the fields inside an interferometer.
- [14] All of the fits used the following parameters: $\lambda_{p(s)} = 532\text{nm}$ (683nm), $\alpha = 3.45 \times 10^{-9} \text{ cm/W}$, $R_{p(f)} = R_{p(b)} = 0.99980$, $R_{s(f)} = R_{s(b)} = 0.99977$, $T_{p(f)} = 156 \text{ ppm}$, $\ell = 7.68 \text{ cm}$, $\beta = 0.001$ (for equation 13), $b = 18 \text{ cm}$. The equations were integrated numerically using the Bulstoer algorithm.
- [15] In order to conserve energy the areas for the pump and Stokes beams, used to calculate power, need to be identical and are normalized to the pump beam. The wavelength dependence of the area for the Stokes beam is included in the mode filling parameter of reference 11.
- [16] J. L. Hall, and T. W. Hänsch, Opt. Lett., **9**, 502 (1984).
- [17] This is the optical power that is coupled into the TEM₀₀ mode of the HFC, the actual power at the entrance of the cavity was 1.1mW
- [18] The measured photon conversion efficiency is smaller than the efficiency reported in reference 1 due to additional exposures to atmospheric conditions. Which increases the absorption of the mirrors of the high finesse cavity.
- [19] The values for the pump and Stokes mirror reflectivities were measured by a cavity ring-down. The values are $R_{p(s)} = 0.99979 \pm 0.00001$ (0.99977 ± 0.00001). The transmissions were $T_p = (153 \pm 8) \text{ ppm}$, and $T_s = (150 \pm 20) \text{ ppm}$.

- [20] W. K. Bischel and M. J. Dyer, Phys. Rev. A., **33**, 3113 (1986).
- [21] The calculated value for the plane-wave gain coefficient is 2.94×10^{-9} cm/W and the experimental values are $(2.5 \pm 0.4) \times 10^{-9}$ cm/W. (see W. K. Bischel and M. J. Dyer, J. Opt. Soc. Am. B, **3**, 677 (1986).)
- [22] The absence of the EOM does not affect the cw Raman laser linewidth due to the fact that the narrowed pump linewidth is on the order of ~ 1 kHz, due to instabilities in the HFC, and the Raman linewidth for the vibrational transition is 510 MHz. However, the HFC transforms frequency noise into amplitude noise, so an EOM was added to increase the stability at frequencies near and above the cavity half-width for the RIN measurements.
- [23] Vibrations on the optical table are on the order of $30 \mu\text{g}_{\text{rms}}$ which occur at a frequency of 90 Hz.

Figure Captions:

1. Shows the growth of the pump (solid) and Stokes (dotted) fields as a function of time. A relaxation oscillation occurs at $\sim 12 \mu\text{s}$, but is damped out in one oscillation.
2. Shows a comparison of the predictions of references 2 and 3 (dashed) with the steady-state limit of the presented time-dependent theory (solid). The percent difference of the theories is plotted (dash-dot). On average the theories differ by less than 1 part per 1000.
3. The normalized RINs of the Stokes (dashed) and pump (solid) beams are shown as a function of noise frequency at four times the threshold of the Raman laser.

4. The relaxation oscillation frequency (solid) is shown as a function of pump power. The Stokes cavity linewidth (dashed) is overlaid for reference. The threshold of the Raman laser is $640\mu\text{W}$.
5. The experimental apparatus used to measure the threshold and the RIN of the cw Raman laser is shown.
6. The Stokes output vs. pump power for the cw Raman laser is shown with the theory overlaid. The threshold was measured to be $640\pm 30\mu\text{W}$.
7. The photon number conversion efficiency vs. pump power for the cw Raman laser is shown with the theory overlaid. The maximum photon number conversion efficiency was measured to be $27\pm 3\%$ at 2.6mW of pump power.
8. The RIN for the pump beam is shown before (dash) and after (solid) the HFC as a function of frequency. The calculated shot noise level is added for reference.
9. The normalized Stokes RIN (a) and the normalized pump RIN (b) are shown as a function of noise frequency. Theoretical predictions of equations 13-16 are overlaid (dashed).
10. The measured normalized RINs of the pump (circle) and the Stokes (square) beams at 30kHz as a function of pump power is shown. The data is fit by the time-dependent theory. The pump RIN is reduced by as much as 35dB/Hz for higher pump powers. The threshold of the Raman laser is $640\mu\text{W}$.
11. Experimental apparatus used to measure the free-running linewidth and stability of the cw Raman laser is shown. NB denotes narrow-band.
12. Heterodyne beatnote linewidth measured by a RF spectrum analyzer. The linewidth of the cw Raman laser was measured to be 4kHz .

13. The Allan variance vs. integration time is shown. A peak due to table vibrations is seen to occur at $\sim 100\text{Hz}$.

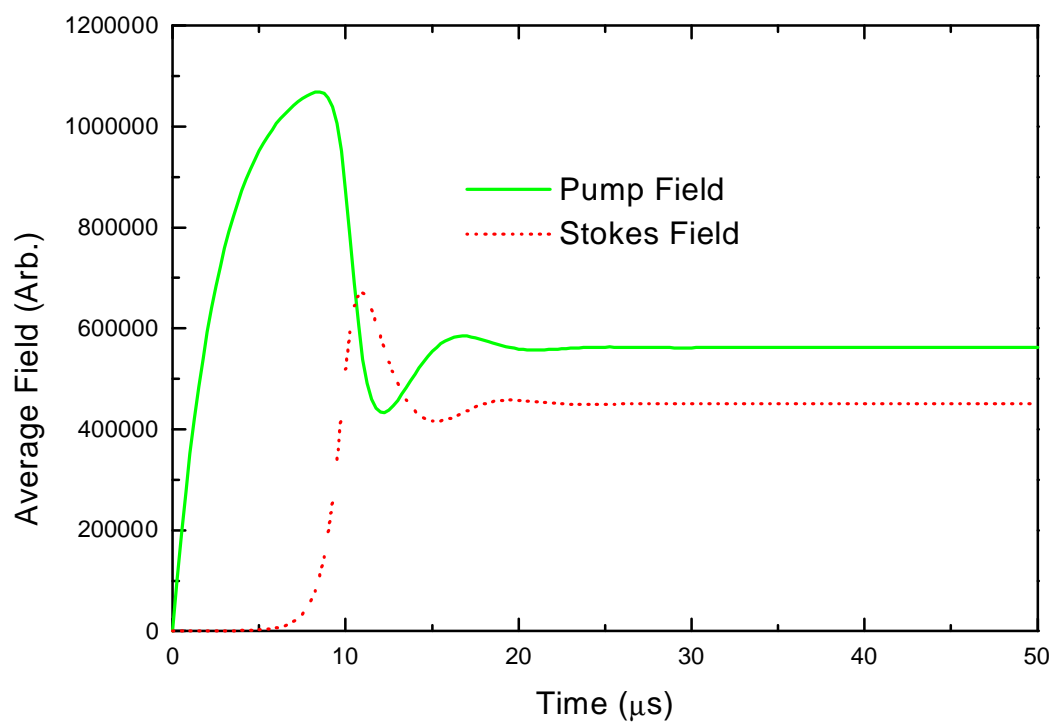


Figure-1

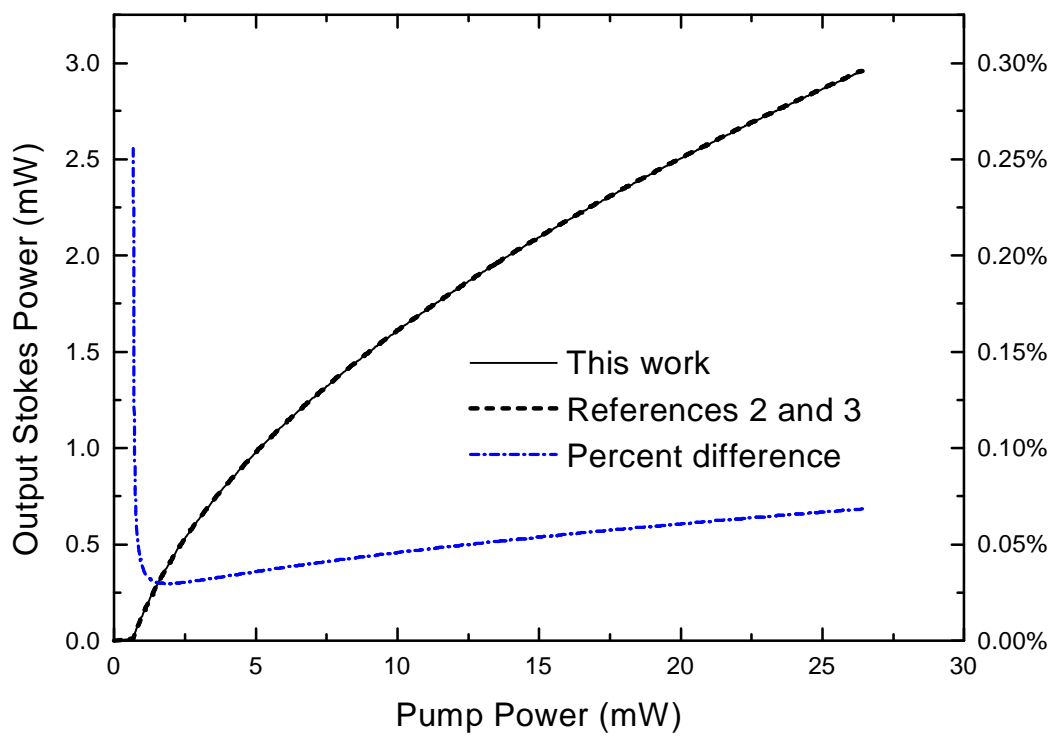


Figure-2

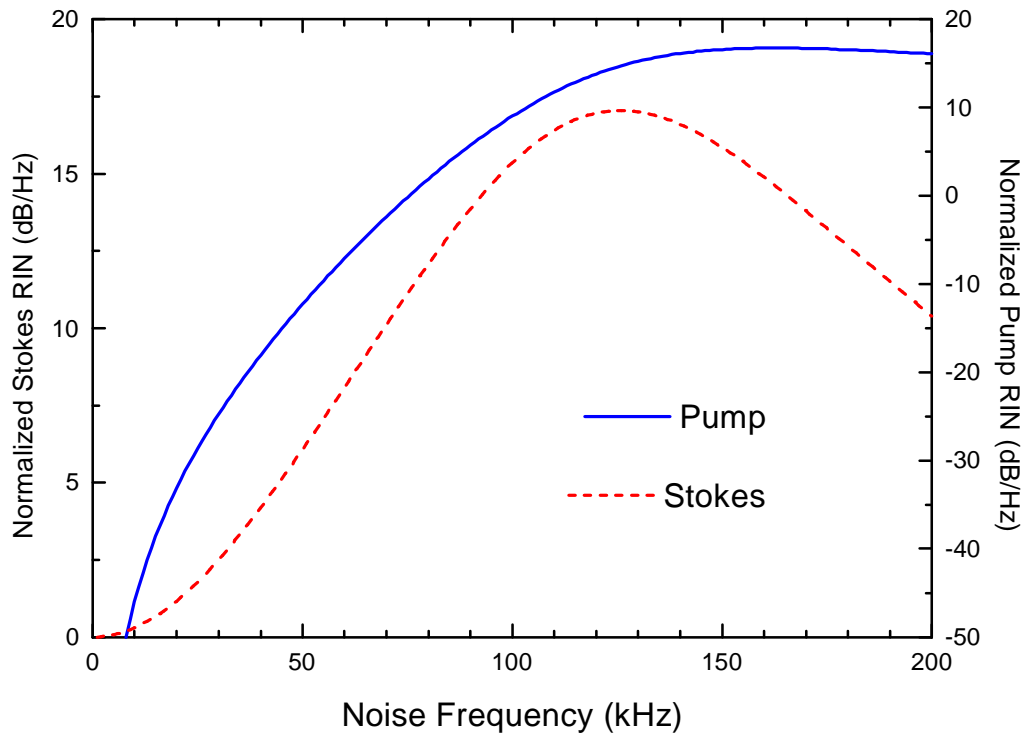


Figure-3

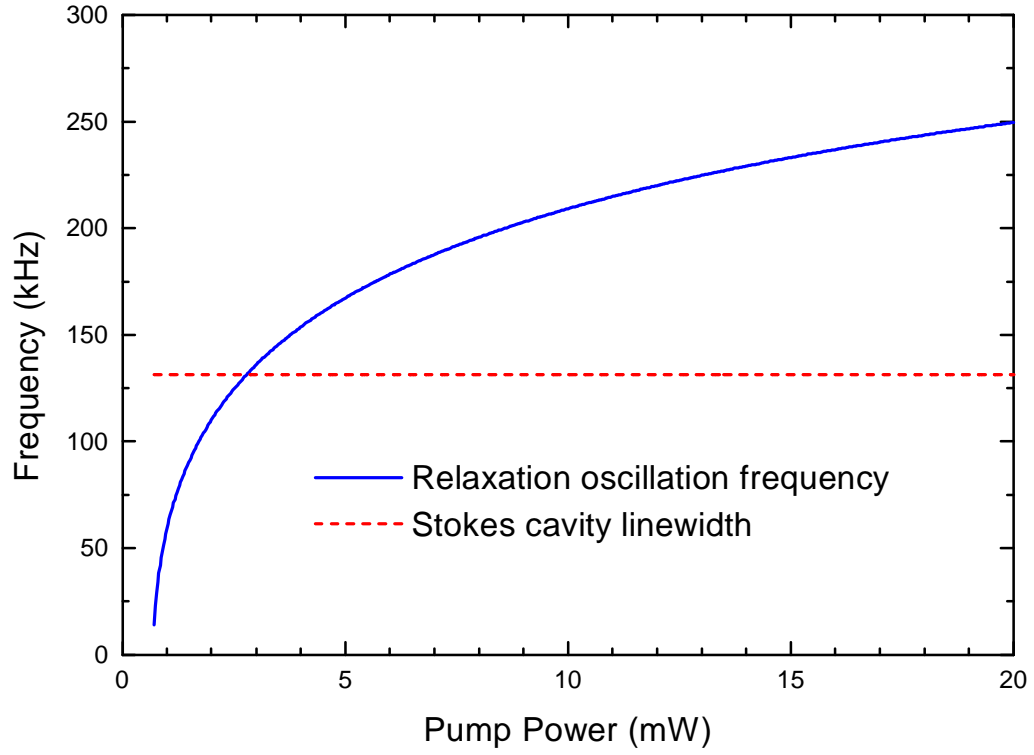


Figure-4

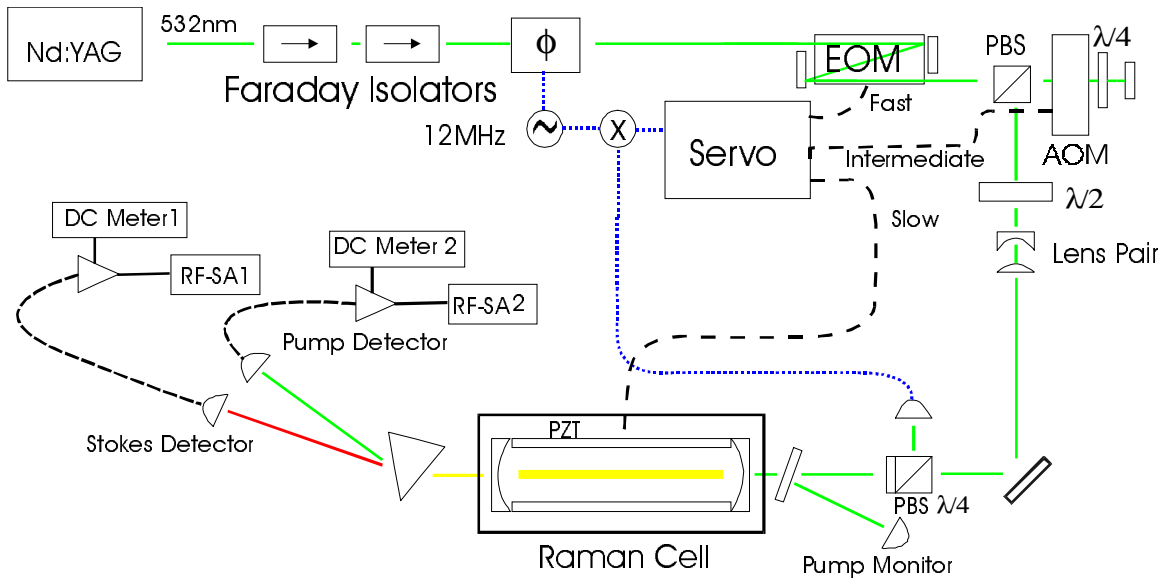


Figure-5

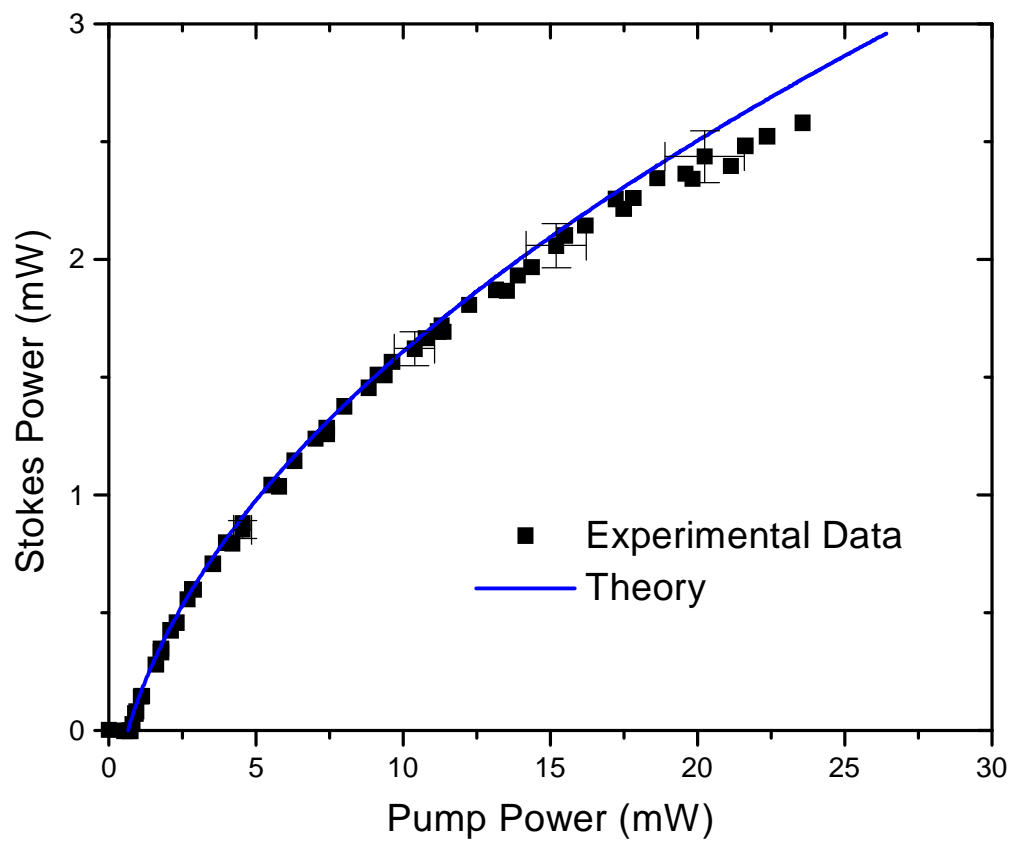


Figure-6

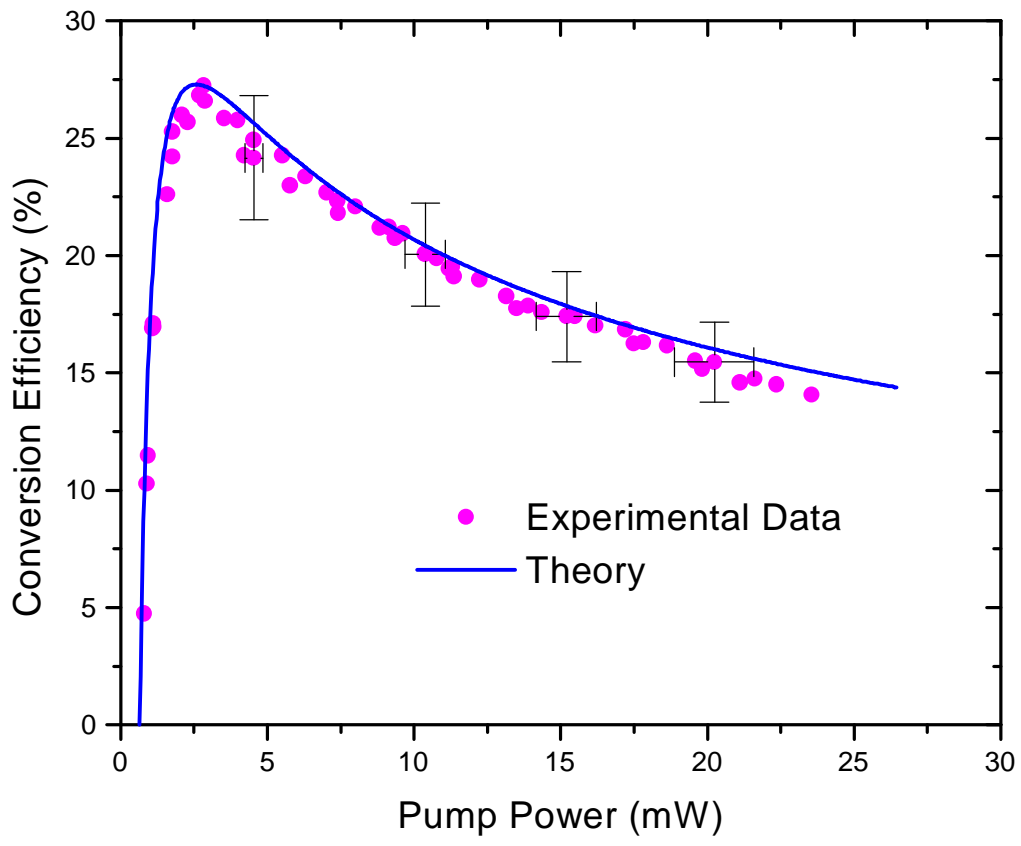


Figure-7

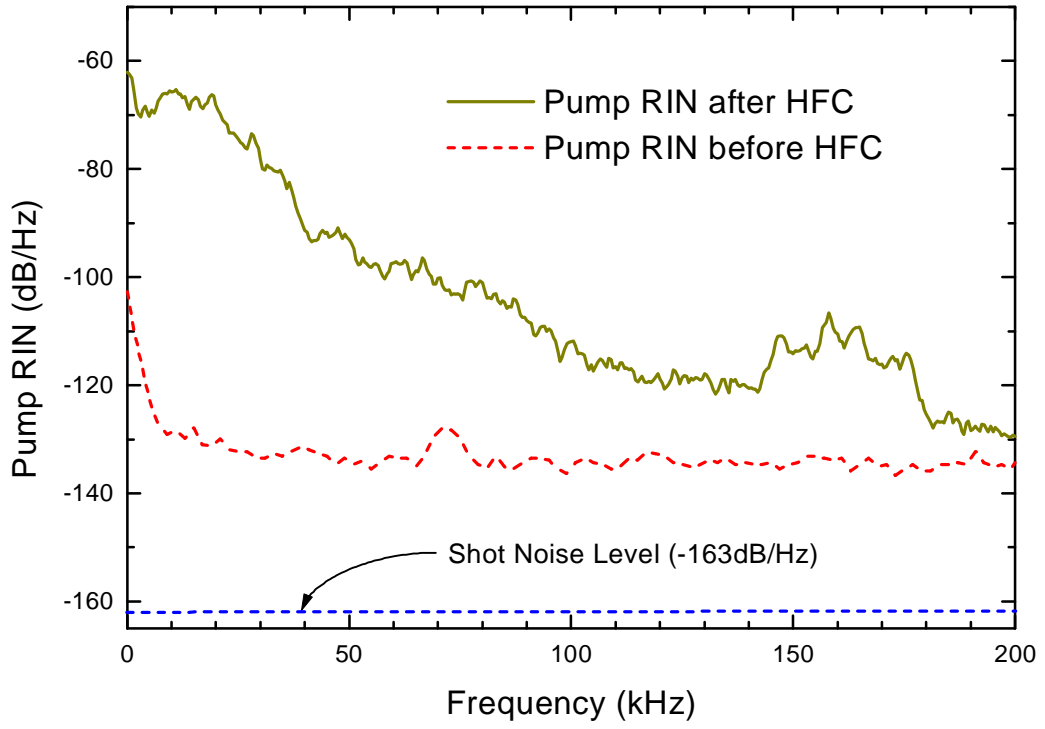


Figure-8

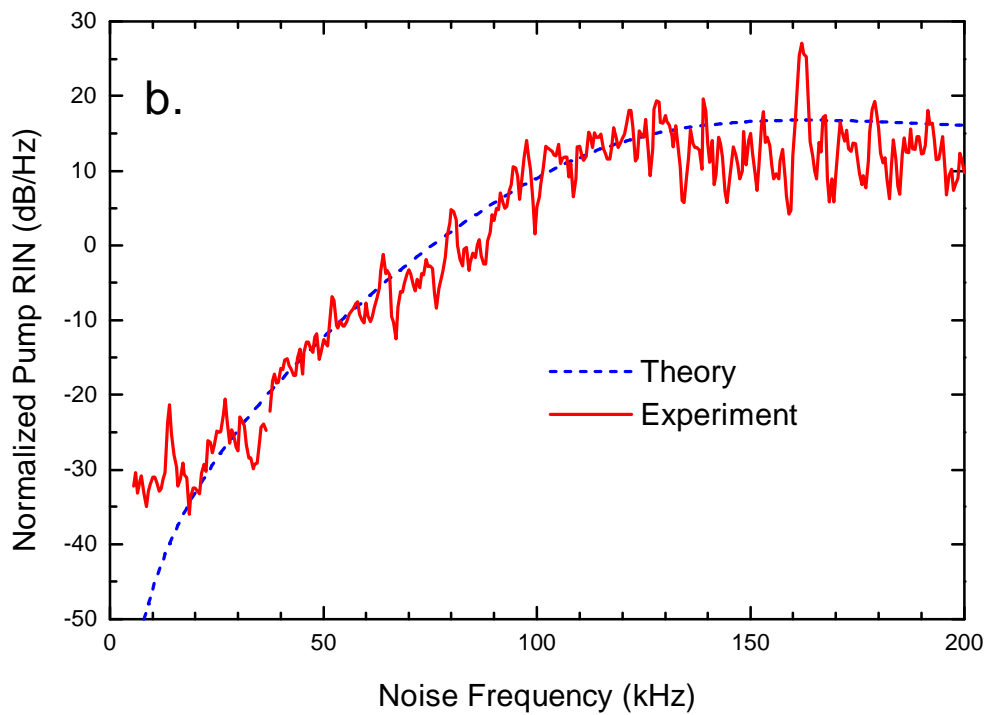
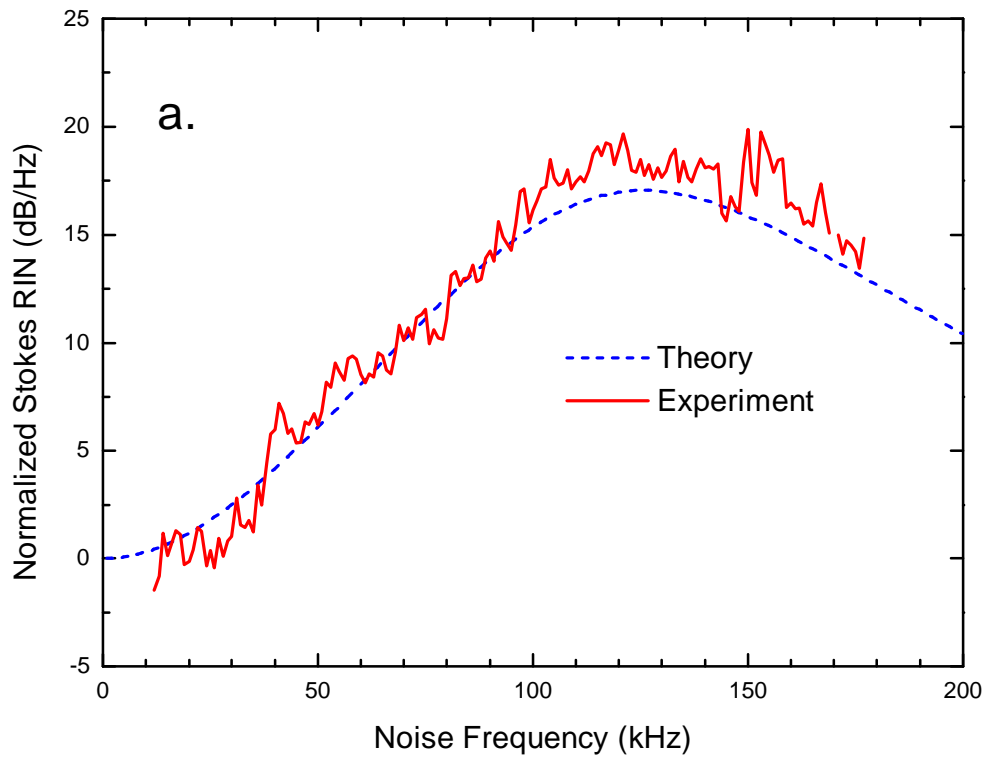


Figure-9

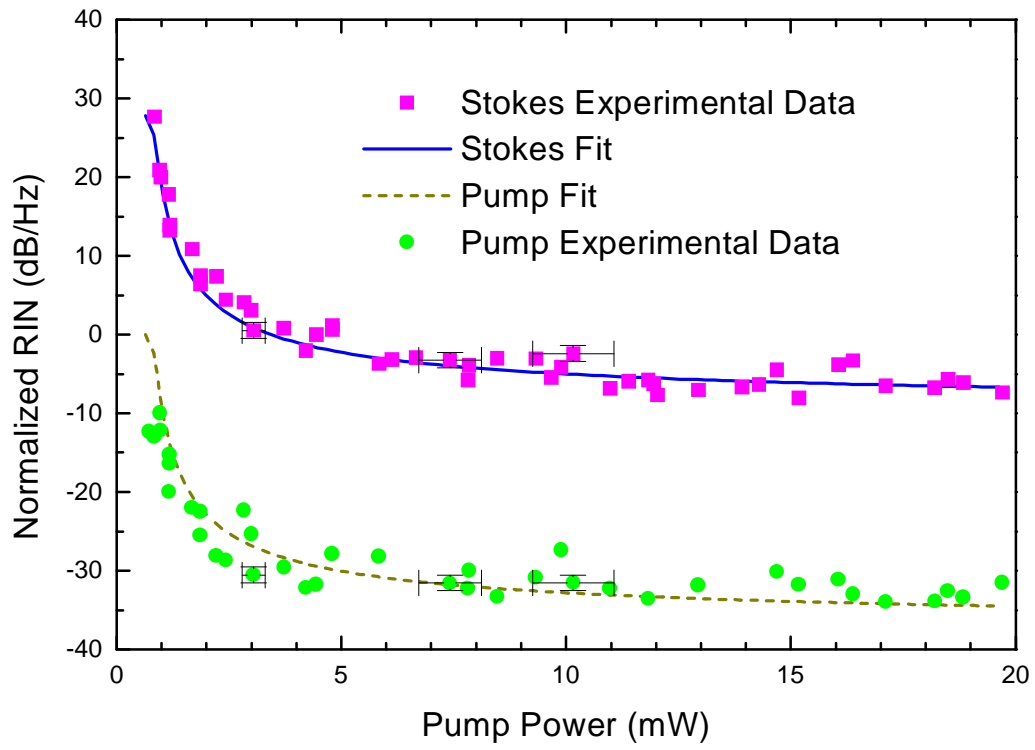


Figure-10

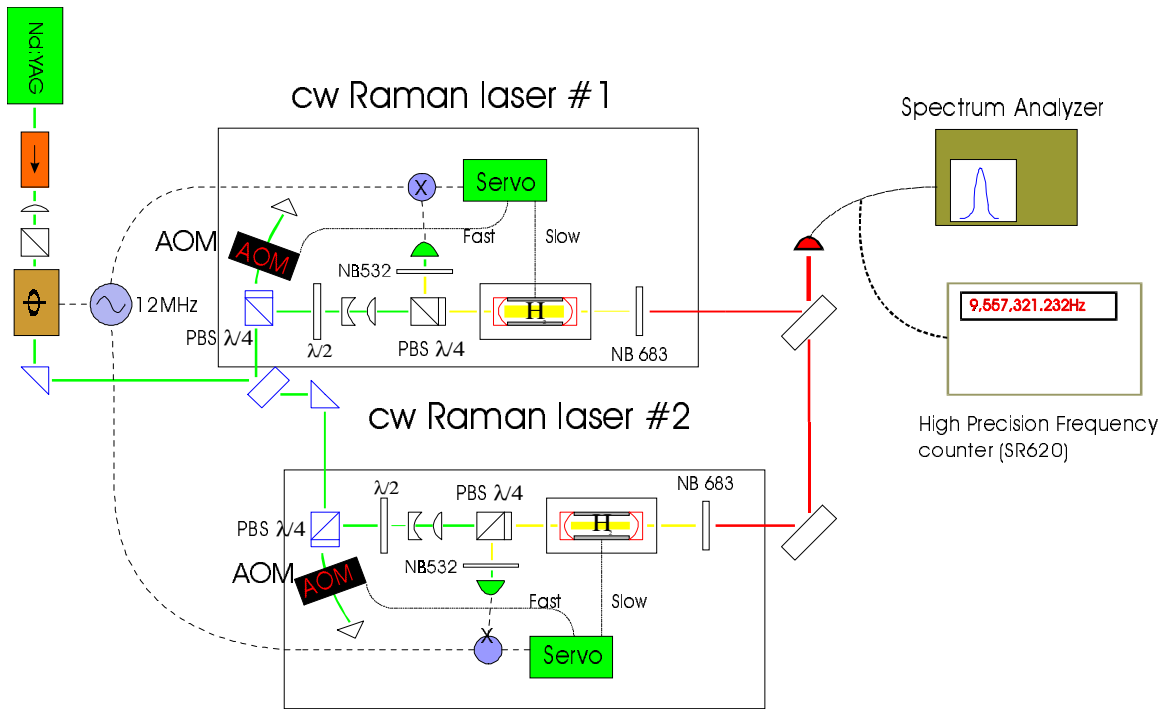


Figure-11

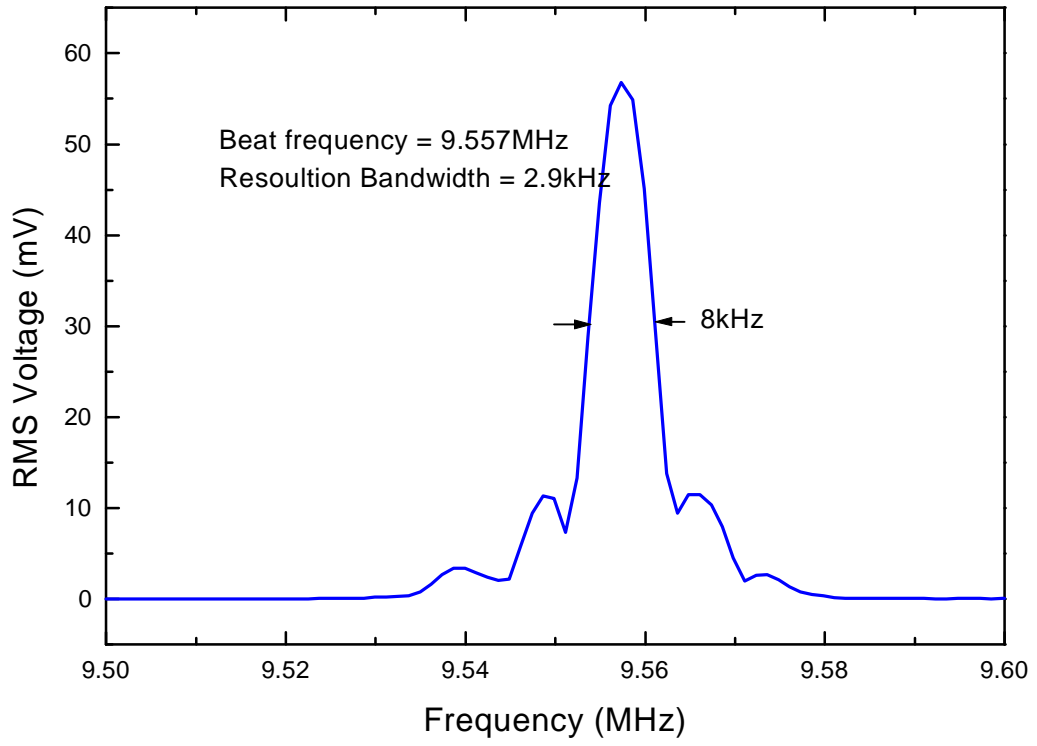


Figure-12

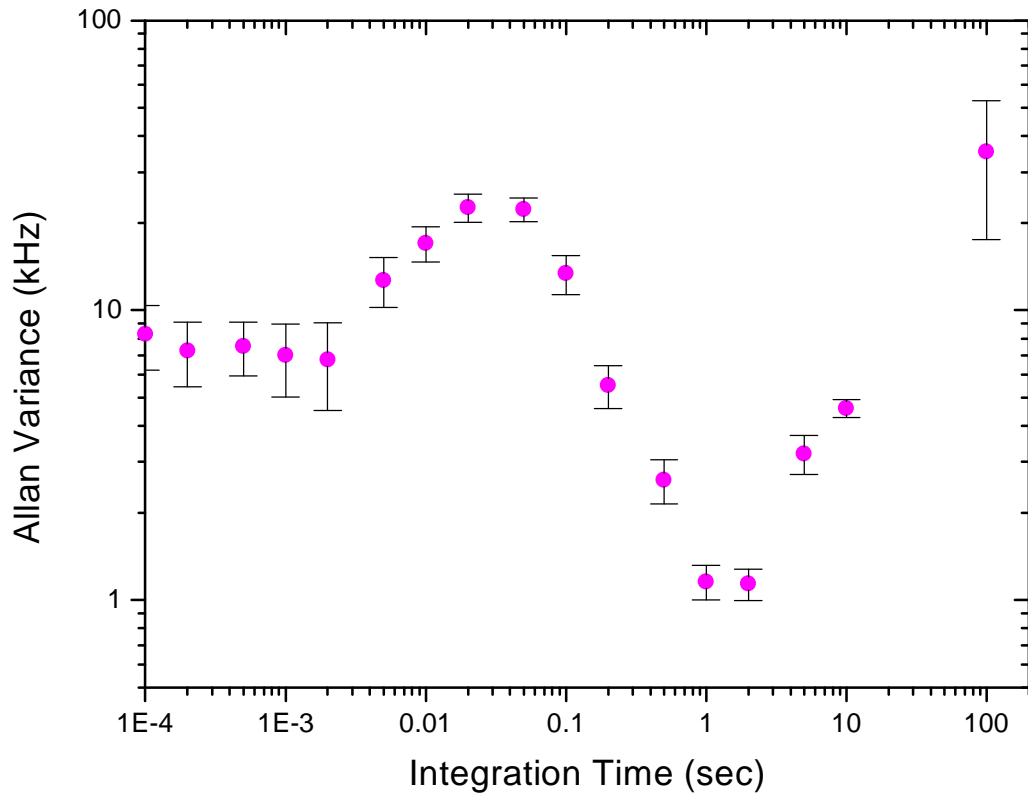


Figure-13